PROCEEDINGS, 51st Workshop on Geothermal Reservoir Engineering
Stanford University, Stanford, California, February 9-11, 2026
SGP-TR-230

Impact of Injection–Production Well Placement on Heat Recovery in Enhanced Geothermal Systems

Jinchuan Hu and Mukul M. Sharma

Hildebrand Department of Petroleum and Geosystems Engineering, Cockrell School of Engineering, University of Texas at Austin, 200 E. Dean Keeton St., Stop C0300, Austin, TX 78712-1585

jchu1006@utexas.edu

Keywords: Enhanced Geothermal Systems, Well Placement, Fracture Propagation, Thermal Recovery, Geomechanics.

ABSTRACT

In Enhanced Geothermal Systems (EGS), the placement of producers relative to injectors can play a very important role in controlling fluid flow patterns, fracture connectivity, and overall energy recovery. Improper placement can result in rapid thermal breakthroughs or reduced heat sweep efficiency. This study aims to (1) investigate how the relative angular alignment of the injector-producer pair influences heat recovery, and (2) provide quantitative design strategies for optimizing well placement to enhance long-term geothermal performance. A fully coupled reservoir-fracture-well simulator that models multi-phase flow, geomechanics, and thermal effects is employed to simulate the fluid circulation process and examine fracture propagation in EGS. It simulates the propagation, opening, and closing of propped fractures under the influence of thermo-poro-elastic stress. The geothermal heat recovery was simulated for different well placements. Changes in flow patterns and fracture geometry over time were analyzed, providing insights into fracture dynamics during geothermal recovery and their impact on overall efficiency. Simulation results demonstrate that well spacing and placement strongly influence heat recovery. Although late-time thermal power converges across all cases, cumulative thermal energy increases significantly with production-well elevation. Larger positive angles enhance buoyancy-driven circulation and sustain heat extraction over longer timescales. These findings highlight the trade-offs in fracture utilization and thermal sustainability, underscoring the importance of carefully selecting well placement strategies in EGS.

1. INTRODUCTION

The escalating global demand for sustainable and reliable energy sources has intensified the search for baseload renewable technologies capable of complementing intermittent sources like wind and solar. Geothermal energy, particularly Enhanced Geothermal Systems (EGS), has emerged as a promising avenue for decarbonizing the global energy sector. The International Energy Agency (IEA) has emphasized the potential of geothermal resources to supply a significant portion of global electricity demand by 2050 under ambitious net-zero scenarios (Bouckaert et al., 2021). Unlike conventional hydrothermal systems, which exploit naturally occurring pockets of steam or hot water, EGS technologies are designed to extract heat from hot, dry rock formations that possess high thermal energy but lack sufficient natural permeability or fluid saturation (Tester et al., 2006; Brown, 2000).

High-profile initiatives, such as the Utah Frontier Observatory for Research in Geothermal Energy (FORGE), serve as critical field laboratories to advance these technologies. As detailed by Moore et al. (2020), FORGE provides a dedicated site to test stimulation protocols in granitic basement rocks, aiming to demonstrate the viability of commercial-scale EGS. However, the commercial success of EGS hinges on creating and maintaining a fracture network that ensures efficient heat exchange without succumbing to common reservoir failures. A primary technical challenge in EGS operation is the management of subsurface fluid flow to prevent "short-circuiting" or thermal breakthrough. Subsurface heterogeneity often creates preferential flow paths—known as "thief zones"—where injected fluid travels rapidly through high-permeability fractures directly to the production well (Willis-Richards and Wallroth, 1995). This phenomenon severely limits the contact time between the fluid and the rock, resulting in uneven heat extraction and a rapid decline in production temperatures, ultimately compromising the economic lifespan of the project (Pruess, 2006).

Compounding this challenge is the complex interplay of Thermal-Hydraulic-Mechanical (THM) processes that govern fracture dynamics. EGS reservoirs are not static; they evolve dynamically in response to fluid circulation. The injection of cold fluid into a high-temperature reservoir induces significant thermal gradients between the fluid and the surrounding rock mass (Ghassemi, 2012). These gradients lead to the thermal contraction of the rock matrix, which generates tensile stresses that can reduce the effective compressive stress acting across fracture faces (Perkins and Gonzalez, 1985). This thermo-poro-elastic coupling can cause existing fractures to open further or propagate, and may even initiate new fractures. As the rock cools, fractures tend to widen, increasing their conductivity and potentially exacerbating flow localization. Numerical simulations and field observations suggest that thermal stresses are often the dominant mechanism driving fracture propagation during long-term circulation, capable of reorienting fracture growth trajectories and altering the connectivity of the reservoir (Ghassemi and Zhou, 2011; McClure and Horne, 2014; Hu et al., 2025; Zhang and Taleghani, 2025). Consequently, understanding the time-dependent evolution of fracture geometry is essential for predicting reservoir performance.

This study employs a fully coupled reservoir-fracture-well simulator to systematically investigate the impact of well placement on heat recovery. We analyze scenarios where the production well is positioned at various angles relative to the injection well, evaluating the effects on fracture propagation, bottom-hole temperature, and cumulative energy extraction over a 10-year period.

2. MATHEMATICAL MODEL

This research utilizes an advanced simulator that comprehensively couples subsurface flow, geomechanics, and energy balance across the reservoir, fracture, and wellbore domains (Hu et al. 2025). The model framework, as shown in Figure 1, detailed by Hu et al. (2023, 2025), incorporates thermo-poro-elastic effects to simulate arbitrary fracture initiation, propagation, and closure.

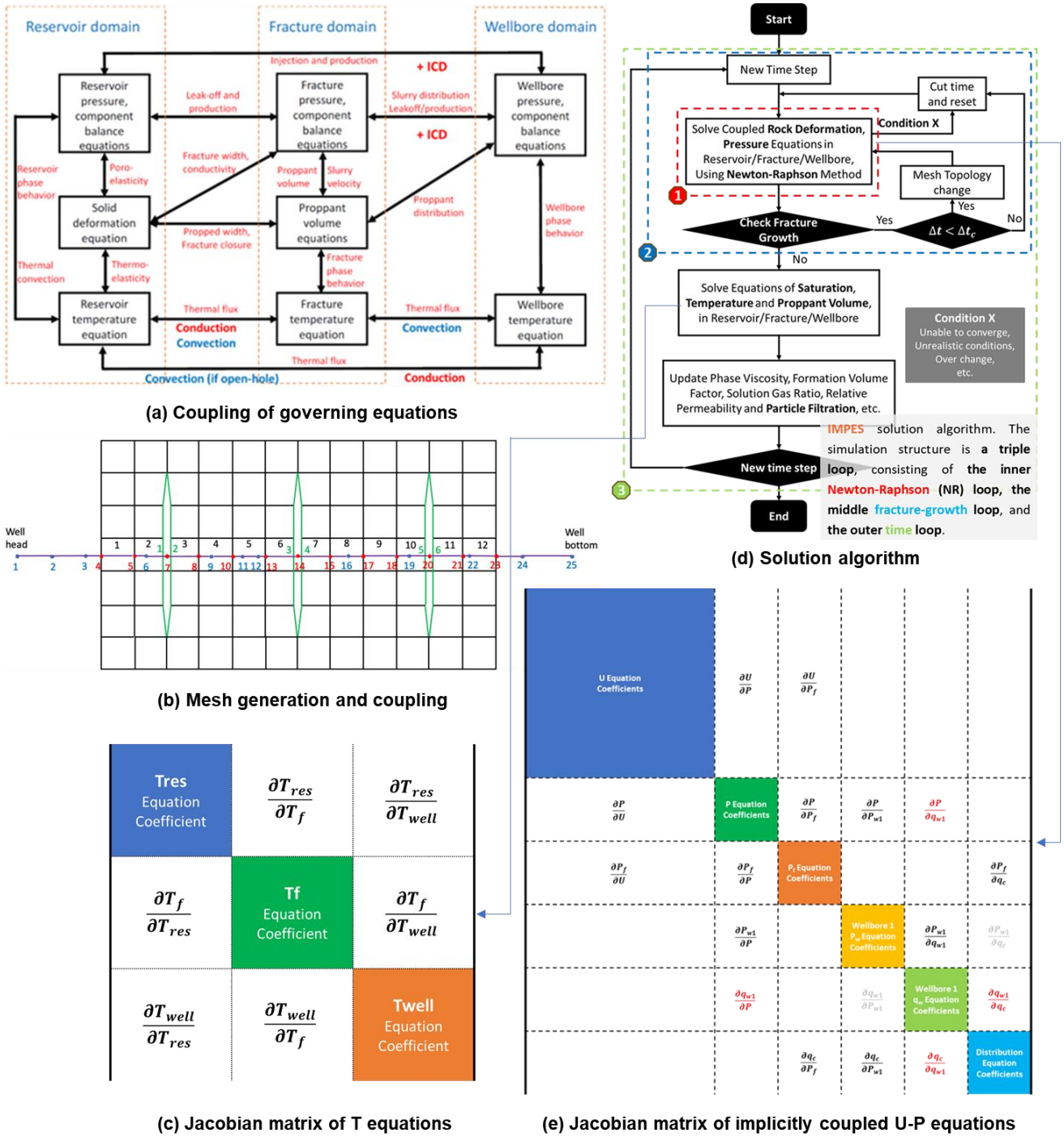

Figure 1: Overview of the simulator: (a) Coupling of governing equations, (b) Mesh generation and coupling, (b) Solution algorithm (IMPES with a triple loop). (c) Jacobian matrix for coupled T equations, (d) Jacobian matrix for implicitly coupled U-P equations. (Hu et al., 2025)

2.1 Solid Deformation and Geomechanics

The solid deformation model integrates linear poroelasticity (Biot, 2004) and thermoelasticity based on Duhamel's principle (Maugin, 2014). Under a tension-positive convention (Coussy, 2004), the governing equilibrium equation for the saturated subsurface porous medium, accounting for pore pressure and thermal stress, is expressed as:

$$\boldsymbol{\nabla} \cdot [G\boldsymbol{\nabla u} + G(\boldsymbol{\nabla u})^T + \lambda \mathbf{I} tr(\boldsymbol{\nabla u}) + \boldsymbol{\sigma_0} - \alpha p \mathbf{I} - 3K\alpha_T(T - T_0)\mathbf{I}] = 0 \tag{1}$$

where, $\boldsymbol{u}$ is the displacement vector, G and λ are Lame parameters, p is fluid pressure in porous medium, $\boldsymbol{\sigma_0}$ the in-situ stress, α is the Biot coefficient, and α_T is the linear thermal expansion coefficient. The term $3K\alpha_T(T - T_0)\mathbf{I}$ represents the thermal stress contribution, which is critical in EGS as the cooling front advances.

Meanwhile, fracture propagation is governed by the cohesive zone model and the stress intensity factor (SIF) criterion. The cohesive zone model (Dugdale, 1960; Barenblatt, 1962) simulates damage and failure using a traction-separation law, while the stress intensity factor determines the propagation path based on maximum tangential stress (Carrier and Granet, 2012; Bryant, 2016). The SIF criterion determines the fracture propagation path based on the maximum tangential stress at the crack tip (Erdogan and Sih, 1963; Malíková, 2015).

2.2 Fluid Flow and Thermal Transport

Accurate modeling of EGS requires accounting for the significant variations in water properties under geothermal conditions. Water density, heat capacity, and viscosity are treated as functions of both temperature and pressure. As temperature decreases from 543 K to 323 K at 25 MPa, water density increases by approximately 26%, and viscosity increases by 463%. These variations induce significant convection and gravity segregation effects. For the flow in fracture, the equation (Zheng and Sharma, 2019) is,

$$\frac{1}{K_f}\frac{\partial p_f}{\partial t} + \frac{1}{V}\frac{\partial V}{\partial t} = \nabla \cdot \left[\frac{w^2}{12\mu}\left(\nabla p_f - \rho g\right)\right] + q \tag{2}$$

where, K_f is the fluid bulk modulus, μ and ρ are the viscosity and density of fluid in the fracture, q is the source/sink term including the cluster flow rate and fluid leak-off rate, p_f, V, w are the fluid pressure, volume and width of the fracture, respectively.

Energy conservation is coupled using a multi-phase thermal model accounting for conduction and convection:

$$\left(\rho_B C_{pB} + \frac{d\left(\rho_B C_{pB}\right)}{dT}\right)\frac{\partial T}{\partial t} - \nabla \cdot \left(k_B \nabla T\right) + \sum_{j=1}^{n_p} \rho_j C_{pj} u_j \nabla T = \sum_{j=1}^{n_p} \rho_j q_j C_{pj}\left(T - T_0\right) \tag{3}$$

where, the bulk heat capacity $\rho_B C_{pB} = (1-\phi)\rho_s C_{ps} + \phi\rho_f C_{pf}$, C_{pj}, C_{ps} and C_{pf} are the specific heat capacity of phase j, the rock and the fluid, and ρ_j, ρ_s and ρ_f are the density of phase j, the rock and the fluid. The bulk thermal conductivity $k_B = \phi \sum_{j=1}^{n_p} k_j S_j + (1-\phi)k_s$, where k_j and k_s are the thermal conductivity for phase j and rock. And u_j is the phase j velocity, T is the recent temperature, while T_0 is the reference temperature. And those in fracture and wellbore are modified based on it.

The mass and energy balances for the reservoir, fracture, and wellbore are coupled together through heat convection between wellbore and fracture, heat conduction and convection between reservoir and fracture, and heat conduction with convection (in an open-hole well) between reservoir and wellbore.

2.3 Numerical Method

The simulator discretizes all governing equations in space using the finite volume method and in time using the backward Euler scheme. To improve numerical accuracy, stability, and computational efficiency, an adaptive time-stepping strategy with automatic error correction and restart capability is implemented.

As illustrated in Figure 1(b), fractures are represented as internal boundaries embedded within the reservoir mesh. The wellbore mesh construction and its coupling with intersecting reservoir and fracture elements follow the methodology proposed by Zheng and Sharma (2019, 2022).

An IMPUEST (Implicit Pressure and Deformation with Explicit Saturation and Temperature) solution strategy is employed, as summarized in Fig. 2(d). The simulator advances in time using a hierarchical triple-loop structure. The inner Newton–Raphson loop solves the fully coupled pressure and geomechanical deformation equations, as Figure 1(e). The intermediate loop updates mesh geometry and accounts for fracture growth and propagation. The outer time loop advances saturation, temperature (as Figure 1(c)), proppant transport, and other evolving state variables, including solution gas ratio and particle filtration effects.

3. CASE SETUP

To isolate the effect of well placement, we simulate a single-fracture system within a domain representative of the Utah FORGE site. The generated fracture is 200 m in length, and 200 m in height initially, in y-z plane, with localized mesh refinement, as shown in Figure 2(a).

The injection well is fixed at the origin (0,0). The production wells are positioned symmetrically at a fixed Euclidean distance (D) of 80 meters from the injector, but its relative angle (A) varies. Four specific well placement configurations were simulated:

1) D80m_A+0°: The production well is at the same depth as the injector (horizontal).
2) D80m_A+30°: The production well is elevated 30° relative to the injector.
3) D80m_A+60°: The production well is elevated 60° relative to the injector.
4) D80m_A+90°: The production well is directly above the injector (vertical).

Figure 2(b) illustrates these relative orientations. And the model parameters are primarily derived from Utah FORGE data, as shown in Table 1. Key parameters include: initial reservoir temperature: 533°K (260°C), injection temperature: 323°K (50°C), rock permeability: 1 μD, Young's modulus: 60 GPa, and simulation Time: 10 years.

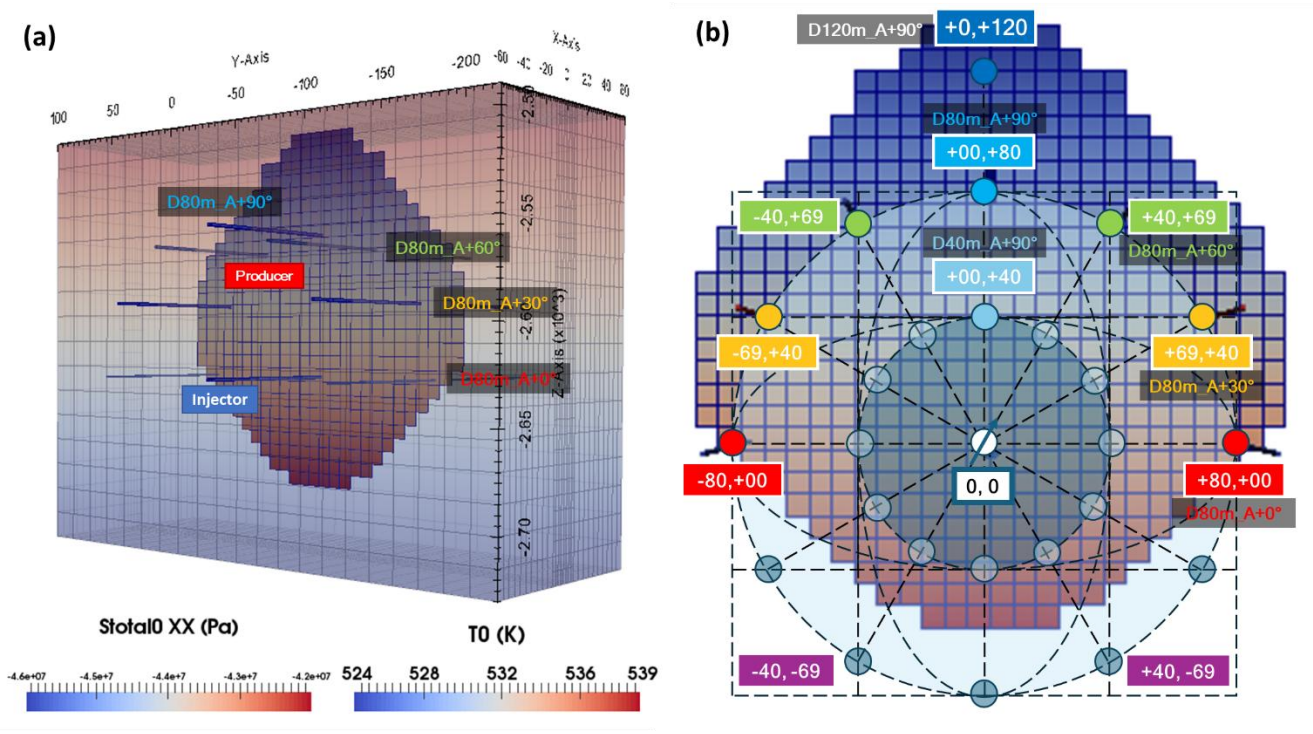

Figure 2: Schematic illustration of (a) three-dimensional numerical model geometry showing the reservoir (colored by the initial minimum total stress, Stotal0 XX), fracture (colored by the initial temperature T0), and well configuration, and (b) the relative orientation of the injection and production wells. The injection well is located at the origin (0,0), and the production well is positioned at a fixed distance D with different relative angles A. The angle A is defined with respect to the injection well, where positive values indicate that the production well is located above the injection well.

Table 1: Input parameters.

Category	Parameter	Value	Unit
Mesh	Dimension (x × y × z)	120 × 315 × 240	m^3
	Maximum grid size	5 × 15 × 15	m^3
	Minimum grid size	1.25 × 3.75 × 3.75	m^3
Reservoir	Porosity	0.01	
	Permeability	1e-3	mD
	Initial pressure at the center	2.535e7 (gradient 8e3/m)	Pa
	Initial reservoir temperature	533 (gradient 0.075/m)	K
Rock	Initial stress at the center (x, y, z)	4.4e7, 4.95e7, 6.4e7	Pa
	Stress gradients (x, y, z)	16965, 26239, 25561	Pa/m
	Thermal expansion coefficient	6e-6	K^{-1}

	Poro-elasticity coefficient	0.48	
	Young's modulus	6e10	Pa
	Poisson's ratio	0.28	
Injection & Production	Injection rate	0.0027 (one fracture)	m^3/s
	Injecting temperature	323	°K
	Producing pressure	2.53e7	Pa

4. RESULTS AND DISCUSSION

To investigate the impact of well placement, we analyzed the evolution of production temperature, thermal power, and cumulative thermal energy in conjunction with changes in fracture geometry and temperature distribution. The results demonstrate that the geometric relationship between the injection and production wells exerts a fundamental control on heat recovery performance in EGS, primarily driven by the interaction between buoyancy forces and thermally induced fracture opening and propagation.

4.1 Production Temperature Dynamics

Figure 3 (left axis) displays the evolution of the Bottom-hole Producing Temperature (BPT) over the 10-year simulation period. A distinct hierarchy in thermal performance is observed based on the angular alignment (A) of the production well relative to the injector.

Horizontal Alignment (A=0°): This configuration exhibits the most rapid and severe thermal breakthrough. The BPT drops sharply within the first 2 years, stabilizing at approximately 410 K. This behavior is attributed to **gravity segregation**. The injected fluid (323 °K) is significantly denser than the initial fluid (533°K). In the horizontal configuration, this cold, dense fluid sinks to the bottom of the fracture and is drawn directly across to the producer, creating a high-permeability, low-temperature channel (or "short-circuit") along the fracture base.

Vertical Alignment (A=90°): In contrast, placing the production well directly above the injection well yields superior thermal performance. The BPT remains above 430 K for the majority of the simulation. By positioning the producer at the top, the system leverages buoyancy differences: the cold injected fluid sinks and accumulates at the bottom of the fracture, away from the production point. To reach the producer, the fluid is forced to sweep upward, contacting a larger volume of hot rock and delaying the arrival of the thermal front.

Intermediate Angles (30°, 60°): The performance improves monotonically with elevation. The 60° case closely mimics the vertical case, suggesting that once the producer is sufficiently elevated above the gravity-driven cold zone, the risk of rapid breakthrough is significantly mitigated.

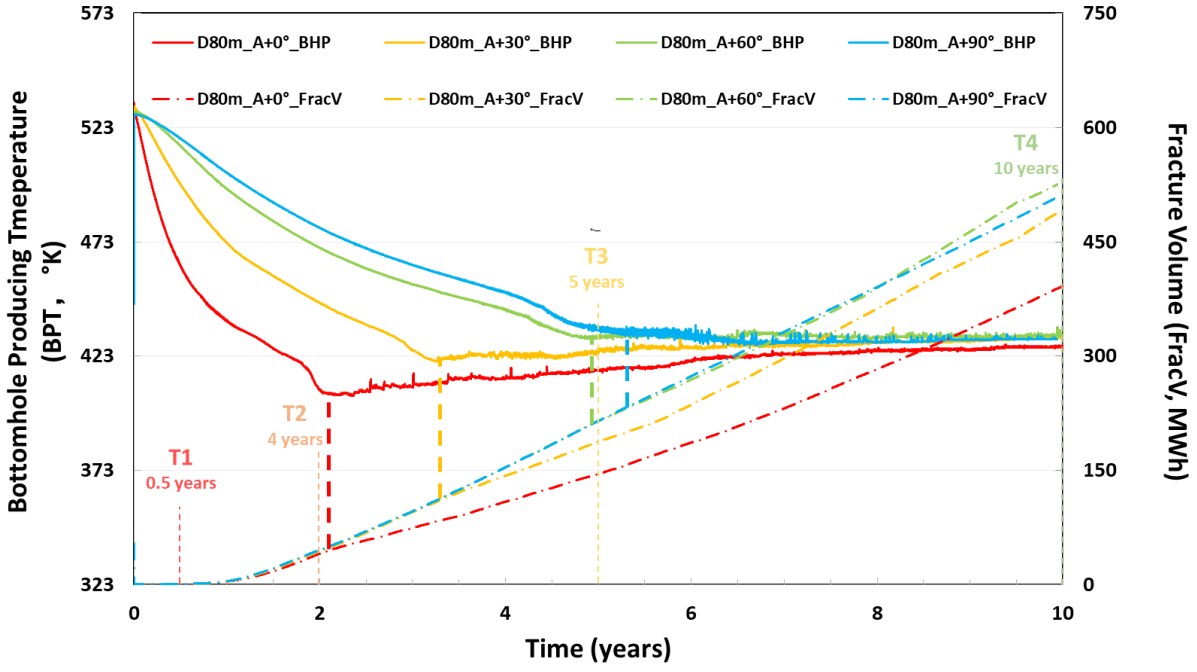

Figure 3: Bottom-hole producing temperature and Fracture Volume over time for different well placement angles.

Hu and Sharma.

4.2 Power and Cumulative Energy

The thermal breakthrough profiles directly dictate the energy extraction efficiency. **Figure 4** presents the Heat Power (HP) and Cumulative Thermal Energy (CTE) profiles.

Power: The power output for the horizontal case (0°) drops below 1,000 kW significantly earlier (around Year 2) than the other configurations. The vertical case (90°) sustains a power output above 1,200 kW for nearly 4 years before entering a gradual decline. Although the heat extraction rate (power) for all cases begin to converge in late time (Year 9-10) as the reservoir cools, the early-to-mid-time performance advantage of the elevated wells is decisive.

Cumulative Energy: The cumulative energy extracted over 10 years quantifies the benefit of exploiting buoyancy. As detailed in **Table 2**, the vertical configuration (90°) recovers **113,504 MWh**, which is **24% higher** than the horizontal baseline (0°). Even a moderate elevation of 30° yields a 12% improvement, while the 60° case achieves a 22% increase. These results underscore that placing producers up-dip is a critical design strategy for maximizing the return on investment in EGS.

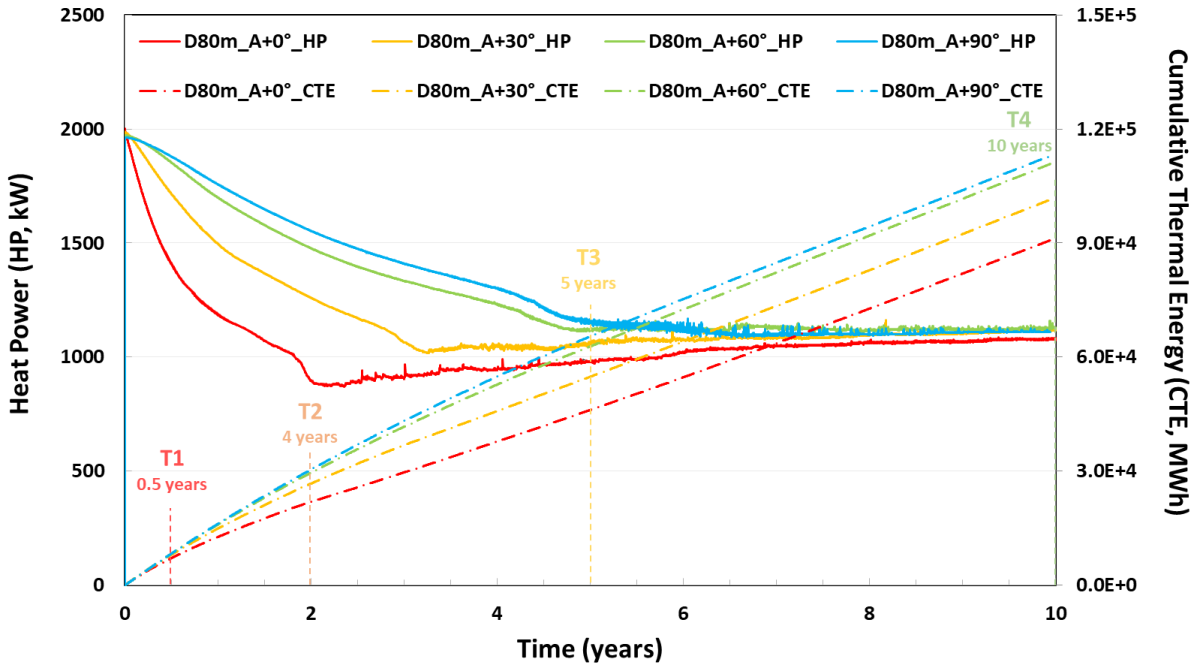

Figure 4: Heat Power and Cumulative Thermal Energy over time for different well placement angles.

Table 2: Cumulative Thermal Energy and relative difference by the end (10 years) for all four cases.

Angle	Cumulative Thermal Energy (CTE, MWh)	Relative difference compared to 0°
0°	91,258	-
30°	101,980	+12%
60°	111,368	+22%
90°	113,504	+24%

4.3 Fracture Geometry Evolution

The injection of cold water induces significant thermal contraction in the rock matrix, reducing the effective compressive stress and driving fracture propagation. **Figure 5** illustrates the evolution of fracture height, length, area, volume, and average width, for different well placement angles.

Fracture Growth: All scenarios exhibit continuous fracture growth after about 1.5 years' circulation, driven by thermo-poro-elastic stresses. However, the extent of growth varies by placement. The 90° and 60° cases achieve larger final fracture areas (>44,000 m^2) compared to the 0° (approx. 42,000 m^2).

Propagation Mechanism: The sinking cold fluid concentrates thermal stress reduction at the bottom of the fracture, driving propagation primarily downward. However, a critical feedback loop exists between sweep efficiency and fracture growth. In the horizontal case (0°), the sweep efficiency is poor (channeling); consequently, less total heat is extracted, and the average rock temperature decreases less across the entire fracture face. This reduced cooling results in a smaller magnitude of thermal stress reduction, leading to less fracture opening and propagation. Conversely, the vertical case (90°) enforces a better sweep, cooling a larger volume of rock. This extensive cooling generates widespread stress reduction, facilitating greater fracture propagation and opening, which in turn exposes more surface area for heat exchange.

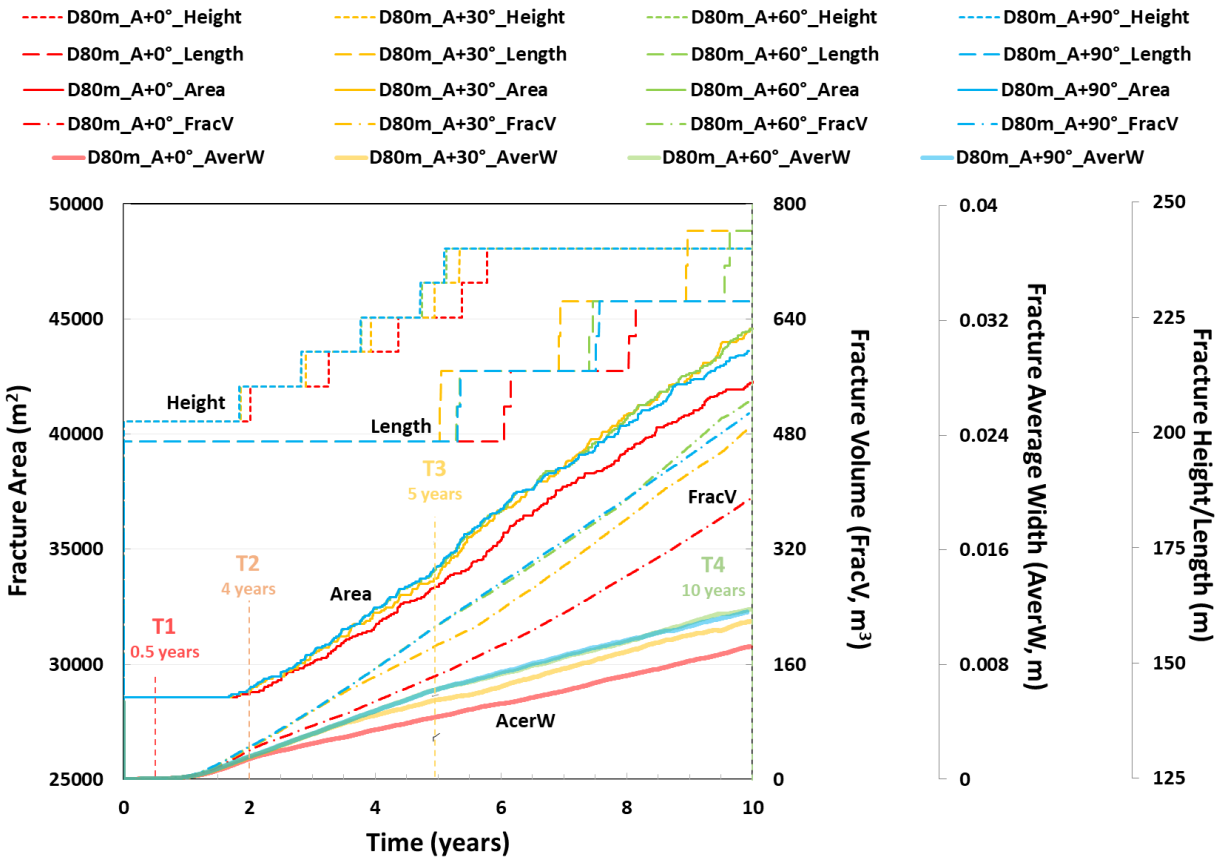

Figure 5: Evolution of fracture height, length, area, volume, and average width, for different well placement angles.

4.4 Flow Visualization and Thermal Sweep

The evolution of the reservoir state is visualized in **Figure 6**, which presents the fracture geometry and temperature distribution for all four cases at t=180, 720, 1800, 3600 days. In these plots, the color represents the temperature distribution (blue indicating cooled regions, red indicating initial reservoir temperature), while the contour lines represent a log-scale fracture width.

Correlation of Width and Temperature: The overlay of width contours on the temperature map highlights the thermo-poro-elastic coupling. Areas of significant cooling (blue zones) coincide with the regions of largest fracture aperture (dense contours). This confirms that thermal contraction is the primary driver for fracture opening, creating high-conductivity pathways within the cooled zones.

Channeling (Horizontal Case, 0°): As early as t=720 days, a distinct cooled channel forms along the bottom of the fracture, connecting the injector directly to the producer. The width contours indicate that this basal channel has the highest conductivity, exacerbating the "short-circuit" effect. By t=3600 days, while the bottom is thoroughly swept and widened, the upper regions of the fracture remain largely hot and relatively narrow, indicating poor sweep efficiency.

Volumetric Sweep (Vertical Case, 90°): In the vertical configuration, the cooled zone (and the associated widened fracture region) expands both radially and vertically over time. Gravity segregates the densest cold fluid to the bottom, forming a "cold pool" away from the production point. To reach the production well located at the top, the fluid must sweep through the warmer rock above. This results in a more uniform transition of temperature and fracture width across the entire fracture face by 10 years, maximizing the heat exchange surface area.

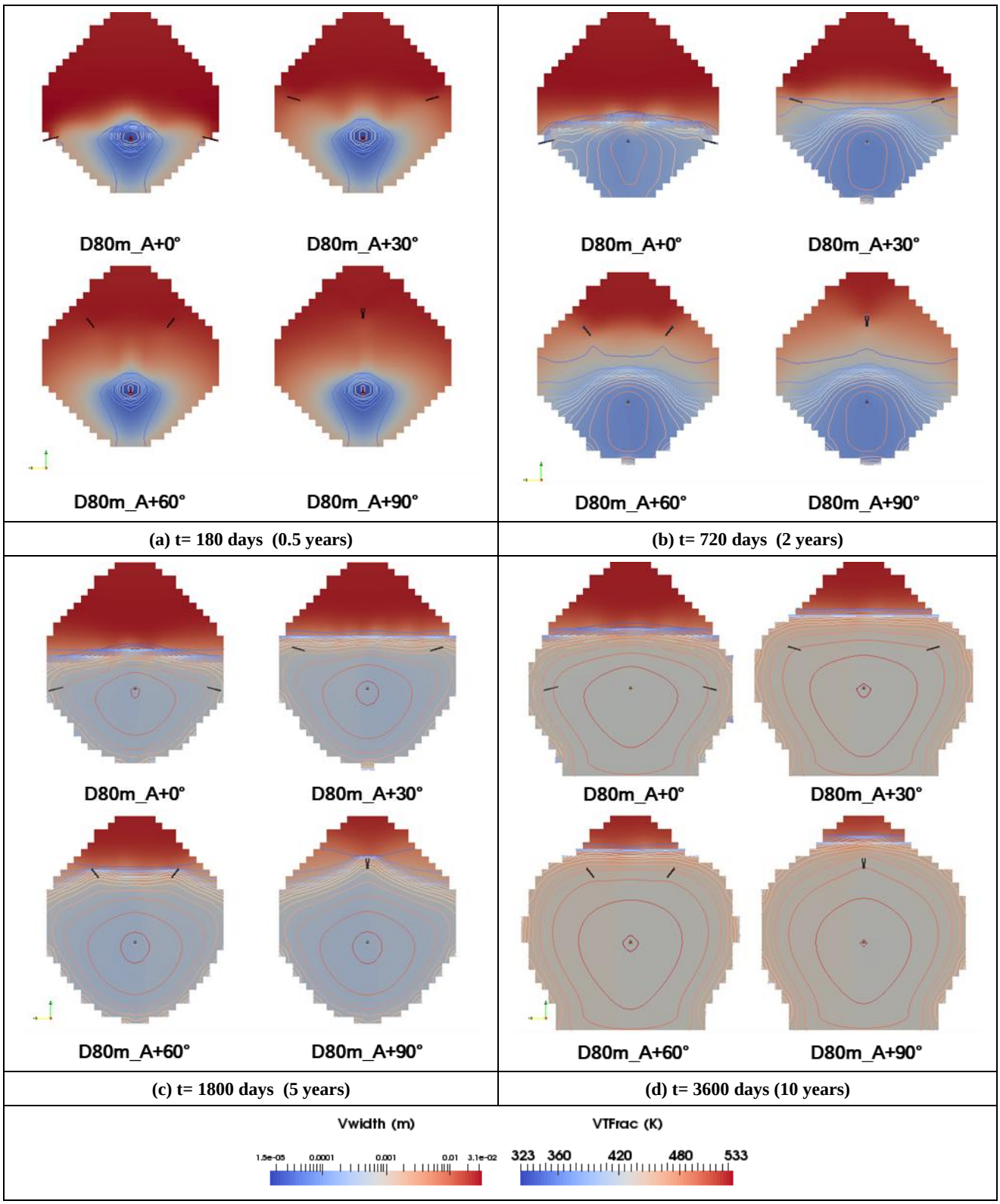

Figure 6: Fracture geometry with temperature distribution for all four cases at t=180, 720, 1800, and 3600 days (the contour lines represent the log-scale fracture width, while the filled color illustrates the temperature distribution).

5. CONCLUTION

This study systematically evaluated the impact of injection and production well placement on heat recovery in Enhanced Geothermal Systems. By employing a coupled thermo-poro-elastic simulator that accounts for dynamic fracture propagation and temperature-dependent fluid properties, we derived the following conclusions:

1. **Placement Sensitivity:** Heat recovery in EGS is highly sensitive to the relative angular alignment of the well pair. The common assumption of horizontal well doublets (0° alignment) may be suboptimal due to gravity segregation effects.

2. **Gravity Dominance:** Gravity segregation is a dominant mechanism. Cold injected fluid is significantly denser than reservoir fluid, leading to rapid sinking. In horizontal arrangements, this leads to basal channeling and early thermal breakthrough.

3. **Optimal Configuration:** Symmetrical placement of the production well vertically above the injection well (+90°) is the most favorable configuration. It yields the highest bottom-hole production temperatures and delays thermal breakthrough most effectively.

4. **Quantitative Benefit:** Elevating the production well provided substantial energy gains. The vertical configuration recovered **24% more cumulative thermal energy** than the horizontal configuration over 10 years.

5. **Fracture Dynamics:** Well placement influences fracture propagation. Vertical flow promotes fracture growth and results in a larger total fracture surface area, further enhancing heat exchange.

These findings suggest that EGS field designs should prioritize "stacking" wells or placing producers up-dip from injectors to leverage natural buoyancy, mitigate channeling, and maximize the return on investment.

REFERENCES

Barenblatt, G.I.: The Mathematical Theory of Equilibrium Cracks in Brittle Fracture, *Advances in Applied Mechanics*, 7, (1962), 55–129.

Biot, M. A.: General Theory of Three-Dimensional Consolidation, *Journal of Applied Physics*, **12** (2), (2004), 155–64.

Bouckaert, S., Pales, A.F., McGlade, C., Remme, U., Wanner, B., Varro, L., and Spencer, T.: Net Zero by 2050: A Roadmap for the Global Energy Sector, *International Energy Agency*, (2021).

Brown, D. W.: A hot dry rock geothermal energy concept utilizing supercritical CO2 instead of water, *Proceedings of the twenty-fifth workshop on geothermal reservoir engineering*, Stanford University, (2000).

Bryant, E.C.: Hydraulic Fracture Modeling with Finite Volumes and Areas, Thesis, University of Texas at Austin, (2016).

Carrier, B., and Granet, S.: Numerical Modeling of Hydraulic Fracture Problem in Permeable Medium Using Cohesive Zone Model, *Engineering Fracture Mechanics*, 79, (2012), 312–328.

Coussy, O.: Poromechanics, *John Wiley & Sons*, (2004).

Dugdale, D. S.: Yielding of Steel Sheets Containing Slits, *Journal of the Mechanics and Physics of Solids*, **8** (2), (1960), 100–104.

Erdogan, F., and Sih, G.C.: On the Crack Extension in Plates Under Plane Loading and Transverse Shear, *Journal of Basic Engineering*, 85(4), (1963), 519–525.

Ghassemi, A.: A review of some rock mechanics issues in geothermal reservoir development, *Geotechnical and Geological Engineering*, **30**, (2012), 647-664.

Ghassemi, A., and Zhou, X.: A Three-Dimensional Thermo-Poroelastic Model for Fracture Response to Injection/Extraction in Enhanced Geothermal Systems, *Geothermics*, 40(1), (2011), 39-49.

Hu, J., Ou, Y., Zheng, S., Sharma, M., Clemens, T., & Chiotoroiu, M. M.: Performance of Inflow Control Devices (ICDs) in Horizontal Injection Wells with Injection Induced Fractures, *SPE Annual Technical Conference and Exhibition*, (2023).

Hu, J., Ou, Y., Zheng, S., and Sharma, M.: Performance of Flow Control Devices (FCDs) in Fractured Horizontal Wells for Enhanced Geothermal Systems (EGS), Proceedings, *Unconventional Resources Technology Conference*, Houston, TX (2025), URTeC 4221594.

Hu, J., Ou, Y., Mura, M., and Sharma, M.: Impact of Thermal Stresses Induced by Fluid Circulation on Fracture Geometry and Heat Recovery Rate in Enhanced Geothermal Systems, *ARMA*, **25-592**, (2025).

Malíková, L.: Multi-Parameter Fracture Criteria for the Estimation of Crack Propagation Direction Applied to a Mixed-Mode Geometry, *Engineering Fracture Mechanics*, **143**, (2015), 32–46.

Maugin, G. A.: Duhamel's Pioneering Work in Thermo-Elasticity and Its Legacy, *Continuum Mechanics Through the Eighteenth and Nineteenth Centuries*, Springer, (2014).

McClure, M.W., and Horne, R.N.: An Investigation of Stimulation Mechanisms in Enhanced Geothermal Systems, International Journal of Rock Mechanics and Mining Sciences, 72, (2014), 242-260.

Moore, J., et al.: The Utah Frontier Observatory for Research in Geothermal Energy (FORGE): A Laboratory for characterizing, creating and sustaining enhanced geothermal systems, *Proceedings of the 45th workshop on geothermal reservoir engineering*, Stanford University, (2020).

Perkins, T.K., and Gonzalez, J.A.: The Effect of Thermoelastic Stresses on Injection Well Fracturing, *Society of Petroleum Engineers Journal*, **25**(01), (1985), 78-88.

Pruess, K.: Enhanced geothermal systems (EGS) using CO2 as working fluid—A novel approach for generating renewable energy with simultaneous sequestration of carbon, *Geothermics*, **35** (4), (2006), 351-367.

Tester, J. W., et al.: The future of geothermal energy, *Massachusetts Institute of Technology*, **358**, (2006).

Willis-Richards, J., and Wallroth, T.: Approaches to the Modelling of HDR Reservoirs: A Review, *Geothermics*, **24**(3), (1995), 307-332.

Zhang, Q., and Taleghani, A.D.: Real-Time Temperature Monitoring and Flow Control for Improved Heat Extraction in Enhanced Geothermal Systems, *Energy*, **314**, (2025), 134274.

Zheng, S., Manchanda, R., and Sharma, M.M.: Development of a Fully Implicit 3-D Geomechanical Fracture Simulator, *Journal of Petroleum Science and Engineering*, **179**, (2019), 758–775.

Zheng, S., and Sharma, M.: Coupling a Geomechanical Reservoir and Fracturing Simulator with a Wellbore Model for Horizontal Injection Wells, *International Journal for Multiscale Computational Engineering*, **20**(3), (2022).